Stretchable Ferroelectric Nanoribbons with Wavy Configurations on Elastomeric Substrates

Xue Feng,[†,#,*] Byung Duk Yang,[‡,#] Yuanming Liu,[§] Yong Wang,[†] Canan Dagdeviren,[‡] Zhuangjian Liu,[⊥] Andrew Carlson,[‡] Jiangyu Li,[§] Yonggang Huang,[∥] and John A. Rogers[‡,¶,*]

[†]AML, Department of Engineering Mechanics, Tsinghua University, Beijing 100084, China, [‡]Department of Materials Science and Engineering, University of Illinois, Urbana, Illinois 61801, United States, [§]Department of Mechanical Engineering, University of Washington, Seattle, Washington 98195, United States, [⊥]Institute of High Performance Computing, A-STAR, Singapore, [∥]Department of Civil and Environmental Engineering and Department of Mechanical Engineering, Northwestern University, Evanston, Illinois 60208, United States, and [¶]Department of Chemistry, University of Illinois, Urbana, Illinois 61801, United States. [#] These authors contributed equally to this paper.

ABSTRACT Applications of ferroelectric ceramics, ranging from components for sensors, memory devices, microelectromechanical systems, and energy convertors, all involve planar and rigid layouts. The brittle nature of such materials and their high-temperature processing requirements limit applications to devices that involve only very small mechanical deformations and narrow classes of substrates. Here, we report a strategy for integrating nanoribbons of one of the most widely used ferroelectric ceramics, lead zirconate titanate, in "wavy" geometries, on soft, elastomeric supports to achieve reversible, linear elastic responses to large strain deformations (*i.e.*, stretchable properties), without any loss in ferroelectric or piezoelectric properties. Theoretical and computational analysis of the mechanics account for these characteristics and also show that the amplitudes of the waves can be continuously tuned with an applied electric field, to achieve a vertical (normal) displacement range that is near 1000 times larger than is possible in conventional planar layouts. The results suggest new design and application possibilities in piezoelectric devices.

KEYWORDS: stretchable electronics · ferroelectrics · nanoribbons · piezoelectrics · energy harvesting

Lead zirconate titanate (*e.g.*, PZT) is one of the most widely used ferroelectric materials, due to its excellent piezoelectric and ferroelectric properties. Many classes of sensors, actuators, and memory elements for use in diverse sectors of industry, ranging from aerospace, automotive, to medicine and microelectronics, rely on PZT.[1−4] A key disadvantage of this material is that it, like most other ceramics, is brittle, and usually fractures at strains that are substantially less than 1%.[5] As a result, devices built with PZT, in conventional layouts and processed using established, high-temperature techniques, can only be subjected to small strain deformations and can be integrated only with narrow classes of substrates. These limitations frustrate many potentially interesting applications, particularly those that require integration with the curvilinear, elastic surfaces of the human body for energy harvesting or health monitoring. The former possibility has recently received significant attention. Flexible devices based on arrays of ZnO nanowires represent one interesting class of technology for this purpose.[6−8] The relative inefficiency of these systems, determined in large part by the poor piezoelectric properties of ZnO, and their restrictive mechanical properties represent two key areas for improvement. Recent reports indicate that the former can be addressed with thin membranes and ribbons of materials such as PZT[9,10] and $BaTiO_3$,[11] created on flat, high-temperature substrates and then integrated with bendable thin sheets of plastic using the techniques of transfer printing. The latter remains an unmet challenge, although a very recent report describes important progress.[12] Advances are needed because devices that offer simple bendability cannot accommodate the shapes and motions characteristic of the human body, that is, curvilinear geometries and large-amplitude deformations.[13] These features demand not only linear, elastic mechanical responses under large strains, but also the ability for conformal integration on surfaces that have arbitrary shapes. In other words, the systems must be able to not only bend, like devices reported previously, but also stretch without fracture or significant degradation in their properties. Here we show that adapted concepts of stretchable electronics[14−18] can be exploited to realize these outcomes with PZT. In particular, we report the fabrication and characterization of structures consisting of nanoribbons of PZT in "wavy", or buckled, configurations on soft, elastomeric substrates. We also introduce a mechanics theory that can

* Address correspondence to jrogers@uiuc.edu, fengxue@tsinghua.edu.cn.

Received for review February 5, 2011 and accepted March 11, 2011.

Published online March 11, 2011
10.1021/nn200477q

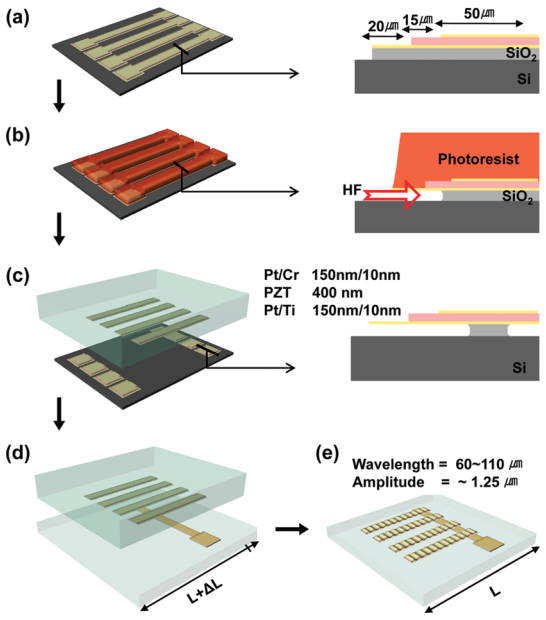

Figure 1. Schematic illustration of procedures for defining PZT devices in nanoribbon formats and for integrating them in wavy configurations on PDMS substrates. (a) Patterning the PZT nanoribbons. The inset provides a cross sectional illustration with representative lateral dimensions. The gold and red layers correspond to the electrodes and the PZT, respectively. (b) Undercutting the sacrificial layer. Photolithographically patterned photoresist protected the PZT layers during removal of the SiO_2 with dilute HF. Etching away the SiO_2 layer underneath the ribbons but incompletely from the pads at their ends prepares the structures for printing. (c) Removing the PZT nanoribbons. The inset shows a cross sectional view and thicknesses for the different layers in the structure. Contacting a PDMS stamp with the PZT and peeling the stamp away removes the ribbons from the silicon wafer and leaves them adhered to the surface of the stamp. (d) Printing the PZT nanoribbons. Aligning a stamp with PZT ribbons to a prestrained substrate of PDMS with a predefined electrode, and then printing transfers the PZT to the PDMS. (e) Forming wavy PZT nanoribbons. Releasing the prestrain leads to a mechanical buckling process that forms wavy structures.

account for the behavior of these systems, including explicitly the effects of piezoresponse. These combined experimental and theoretical results appear to be relevant for a range of applications that cannot be addressed with conventional rigid technologies or with newer ones that offer only bendability.

RESULTS AND DISCUSSION

Figure 1 illustrates schematically a process flow for producing wavy PZT nanoribbons on elastomeric substrates, using ideas originally developed for silicon.[14] The starting structure in this case consists of a bottom electrode of Pt/Ti on an oxidized silicon wafer, with a layer of PZT formed by sol–gel techniques on top. Sputtering and photolithography define top electrodes of Pt/Cr (150 nm/10 nm) with widths of 50 μm. Inductively coupled plasma reactive ion etching (ICP-RIE)[19] through a hard mask of SiO_2 defines the PZT into strips with a thickness of 400 nm, widths of 80 μm, and lengths of 1 mm (see the Experimental Methods section). Another ICP-RIE step patterns the bottom electrode, with a different mask. This process also leaves large square pads (~120 × 120 μm) at the ends of the ribbons. Patterning a layer of photoresist across the entire width of the structure followed by immersion in dilute hydrofluoric (HF) acid completely eliminates the oxide layer under the lengths of the ribbons, but only partially removes this layer from under the pads, due to their larger dimensions. In this way, the ribbons are completely released, but they remain tethered to the underlying wafer due to their connection to these pads. The techniques of transfer printing are used to remove the PZT nanoribbons from the substrate, *via* fracture at points near their ends, and then to deliver them to a prestrained (a few percent, biaxial for cases reported here) slab of the elastomer polydimethylsiloxane (PDMS; Dow Corning). This PDMS substrate supports metal lines and pads with widths of 300 μm that connect to the bottom electrodes on the ribbons. Relaxing the prestrain leads to the spontaneous formation of wavy structures along the nanoribbons, due to nonlinear buckling phenomena of the sort that we have previously studied in silicon.[14–16] The final geometry depends strongly on the prestrain, the flexural rigidity of the nanoribbons, and piezoelectric effects, as described subsequently.

Figure 2a shows a cross sectional scanning electron microscope (SEM) image of the device stack on the silicon wafer, which consists of the top electrode (Pt/Cr), the active material (PZT), the bottom electrode (Pt/Ti), the SiO_2 release layer and the underlying silicon substrate, all with thicknesses consistent with the values reported above. X-ray diffraction (XRD, Philips X'pert) reveals the expected crystal structure in the PZT. As shown in Figure 2b, two main peaks belonging to (100) and (111) PZT are clearly visible. The increased piezoelectric response and poling efficiency at compositions near Zr:Ti = 52:48 are due to the increased number of allowable domain states at the morphotropic phase boundary. Figure 2c presents topographical measurements of the nanoribbons, immediately after the ICP-RIE etching processes but before elimination of the SiO_2, determined using an atomic force microscope (AFM, Asylum Research MFP-3D). These results indicate that most areas are smooth with a root-mean-square (rms) of 21.9 nm. The widths of the top electrodes and the PZT ribbons are 50 and 80 μm, respectively, consistent with the design. Variations in thickness across the ribbon are also apparent, with central regions that are thicker than the edges, as in Figure 2d. This variation results from some undercut removal of PZT near the edges during the etching of the bottom electrode. In particular, the thickness of the structure at the edges is 150 nm, corresponding to the absence of PZT.

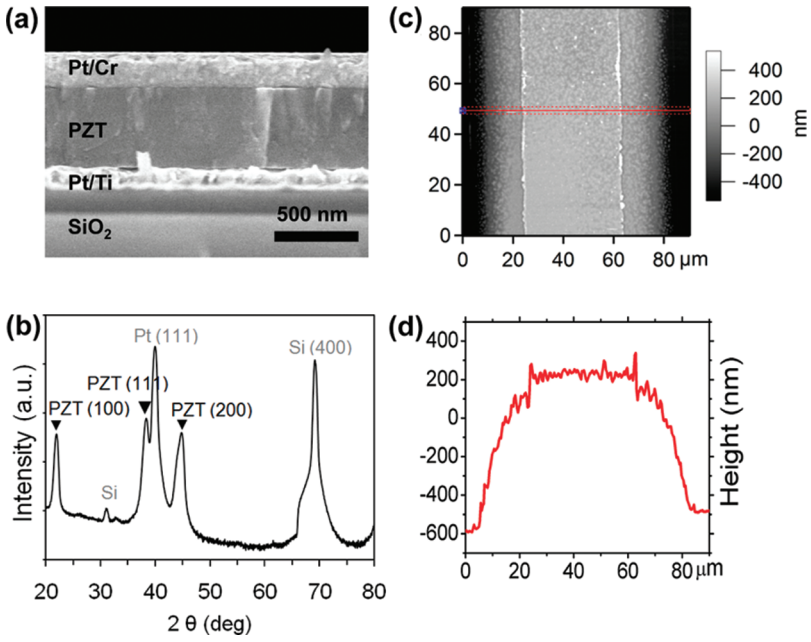

Figure 2. Structural characterization of PZT nanoribbons prior to their integration with PDMS. (a) SEM cross sectional image of the material stack, Pt/Cr/PZT/Pt/Ti, on SiO_2/Si. (b) X-ray diffraction spectrum with PZT peaks labeled. (c) AFM image of PZT nanoribbons with electrodes. (d) Height profile along the ribbon cross section; the red line in frame (c) indicates the approximate position of this profile.

Some representative wavy structures formed by integration with PDMS and release of prestrain (~5%) appear in Figure 3a–c. The flat regions near the right and left edges of the images result from connection to the electrodes on the PDMS (Figure 1).[20] The short period buckling deformations at the edges of each of the ribbons are due to the smaller thicknesses in those regions, as described above (Figure 2c,d). We observe no fracture or cracking of any part of the structures, consistent with the small strains in the materials, as described in more detail subsequently in the context of the mechanics theory where we show that the peak strains are in the range of ~0.3%. We also performed full three-dimensional (3D) modeling using the finite element method (Dassault Systèmes Abaqus) to determine the patterns of buckling when the edge effects associated with undercut etching mentioned above are explicitly included. A solid 3D rendering of the calculated displacements appears in Figure 3c. The overall shapes agree remarkably well with the images in Figure 3a,b. These results confirm that the short period buckling structures at the edges are due to the reduced thicknesses in those regions. Figure 3c also shows a smooth transition from the structures at the edges to the comparatively long period, sinusoidal buckling patterns at the center.

These wavy shapes provide linear elastic responses to applied strain, with a physics that resembles an accordion bellows, as shown in Figure 4. In particular, as the tensile strain increases, the wavelengths and amplitudes of the sinusoidal shapes increase and decrease, respectively. For applied strains comparable

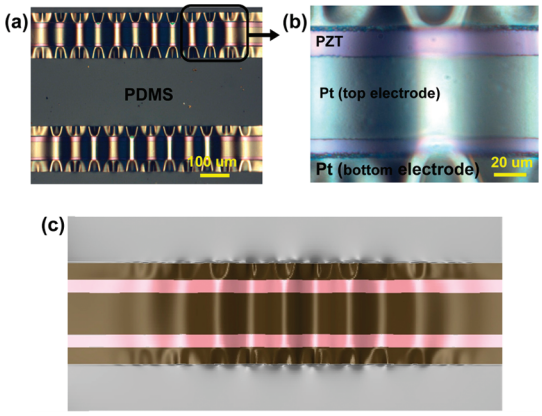

Figure 3. Wavy PZT nanoribbon devices on PDMS, and full three-dimensional (3D) simulations obtained using the finite element method. (a) Optical image of a pair of wavy PZT nanoribbons with electrodes on PDMS. (b) Magnified optical image for a sample similar to the one in (a). (c) Three-dimensional rendering of the calculated displacements for structures identical to those in frame (a).

to the prestrain, the amplitude approaches zero, as seen in Figure 4 inset. Upon release of the applied strain, the structure returns to its original wavy shape, with little or no change. Figure 4 also presents plots of the wavelength, measured by optical microscopy (black square) as well as predicted by the theoretical model (red solid line) as a function of applied tensile strain. The wavelength is related to the prestrain ε_{pre} and applied strain ε_{app} by[16,21] $\lambda = 2\pi h_{stack}[\bar{E}_{stack}/(3\bar{E}_s)]^{1/3}(1+\varepsilon_{app})^{2/3}/(1+\varepsilon_{pre})$, where $h_{stack} = 2h_{Pt} + h_{Cr} + h_{PZT} + h_{Ti}$ (~720 nm) is the total thickness of Pt/Cr/PZT/Pt/Ti stack, $\bar{E}_{stack} = (2\bar{E}_{Pt}h_{Pt} + \bar{E}_{Cr}h_{Cr} + \bar{E}_{PZT}h_{PZT} + \bar{E}_{Ti}h_{Ti})/h_{stack}$

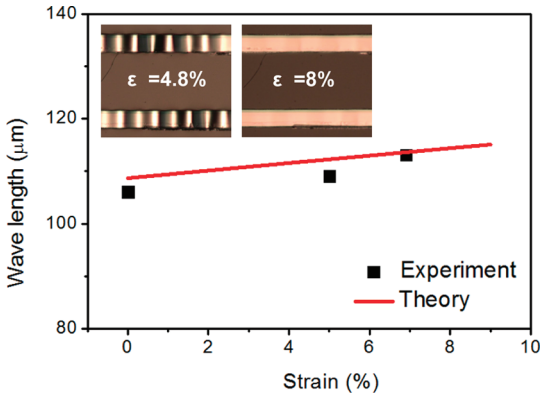

Figure 4. Measured wavelength of wavy PZT nanoribbons as a function of applied tensile strain. The insets show images of wavy PZT nanoribbons subjected to 4.8 and 8% tensile strains. The red line provides prediction based on mechanics theory.

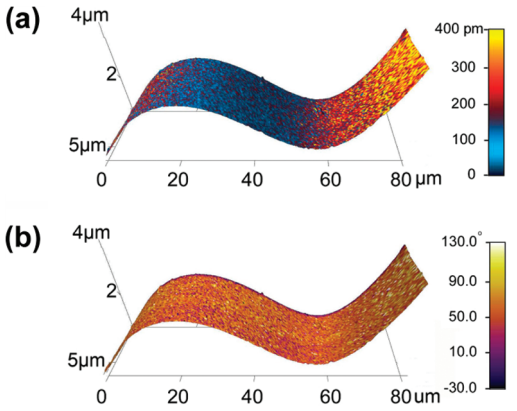

Figure 5. PFM measurement of wavy PZT ribbons with electrodes, for AC voltages at frequencies of 835 ± 10 kHz. (a) PFM amplitude image overlaid on AFM profile; (b) PFM phase image overlaid on AFM profile.

(~143 GPa) and $\bar{E}_s$ (~2.6 MPa) are the effective plane-strain moduli of the stack and substrate, respectively, $\bar{E}_{Pt}$ = 196 GPa, $\bar{E}_{Cr}$ = 292 GPa, $\bar{E}_{PZT}$ = 128 GPa, and $\bar{E}_{Ti}$ = 129 GPa.[22] The theoretical prediction agrees well with the experiment. The lines present expected variations based on the simple physics of an accordion bellows, in which the fractional change in wavelength equals the applied strain.[16] Responses to compressive strains are similar to those of tensile strains, due to the underlying mechanics as described elsewhere.[21] More detailed analysis appears subsequently.

The ferroelectric and piezoelectric properties of these wavy PZT nanoribbons are crucial to their envisioned applications. To examine these aspects, we used piezoresponse force microscopy (PFM) with an atomic force microscope (AFM, Asylum Research MFP-3D). The metal pads that connect to the bottom electrodes serve as electrical ground. An AC driving voltage of 6.6 V applied to the specimen through a conductive AFM tip (Ultrasharp NSC18/Pt/AlBS, MicroMasch) while it scans the specimen surface creates a surface vibration due to the piezoelectric response. This motion allows spatial mapping of the amplitude and phase of the piezoresponse, which correlate to the magnitude and polarity of the piezoelectric coefficient. The use of two AC frequencies of 835 ± 10 kHz near the resonance using a dual frequency resonance tracking (DFRT) technique provides enhanced sensitivity and determination of the quality factor Q simultaneously (~7.7 for the cases reported here). The resulting amplitude and phase maps, overlaid on the AFM topography profiles for a single period in a representative wavy structure, appear in Figure 5a,b, respectively. From the topography, the half wavelength and the amplitude of the wavy structure in this case are ~53 and ~1.25 μm, respectively, consistent with prediction (Figure 4). The piezoresponse varies in a non-uniform fashion, with a maximum response of ~400 pm. For Figure 5a, the area near the left wave peak (blue) corresponds to a minimum. Approaching the right wave peak, the piezoresponse increases gradually and finally reaches a maximum. These variations correlate to local deformations associated with the wavy morphology. Moreover, strain gradients exist both along the ribbon thickness (*e.g.*, top surface in tension and bottom surface in compression, due to bending) and length (*e.g.*, top surface of crests and troughs in tension and compression, respectively) directions. As a result, piezoelectric effects induced by both the local strain[1] and the strain gradient (*i.e.*, flexoelectric)[23] contribute to variations in the piezoresponse.

To investigate the ferroelectricity of the PZT nanoribbons, a sequence of DC biases were imposed on top of the AC driving voltage, with the piezoresponse measured simultaneously. The results are characteristic phase−voltage hysteresis loops and amplitude−voltage butterfly plots. The hysteresis exhibits well-defined, symmetric "square" behavior, as in Figure 6a. The amplitude response presents an expected "butterfly" curve, shown in Figure 6b. Both phase and amplitude results are consistent with bulk PZT materials,[24,25] thereby suggesting that ferroelectric domains with polarization exist and are capable of switching in the wavy nanoribbon layouts. Comparison of the effective piezoelectric coefficient d_{33} before and after transfer printing can be performed by statistically mapping the measured hysteresis and butterfly loops for these two cases, as shown in Figure 6c. The hysteresis loops are symmetric with respect to the applied voltage, and the piezoresponse of the wavy PZT nanoribbon on PDMS is comparable to that of a corresponding flat film on the silicon substrate in magnitude, with slightly bigger coercive field perhaps due to small bending strains associated with the wavy forms. Overall, the results confirm that the processing of Figure 1 does not degrade ferroelectric and piezoelectric properties.

The experimental results collectively suggest that wavy nanoribbons of PZT on PDMS have potential as a

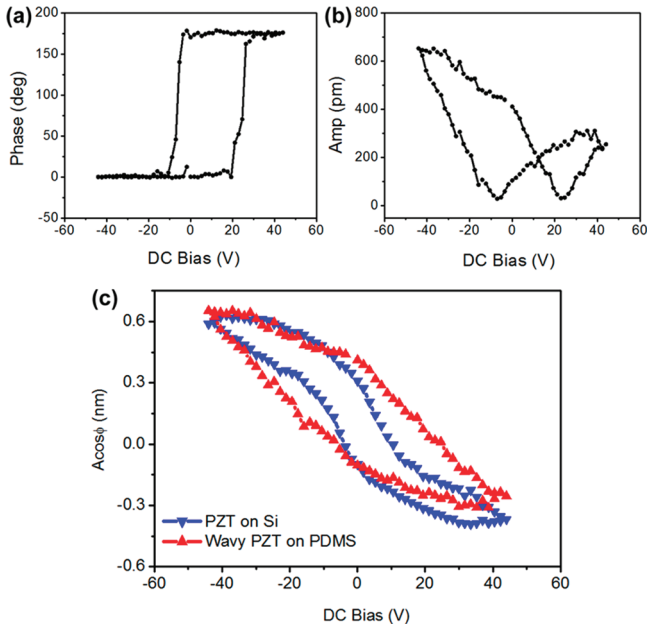

Figure 6. (a) PFM hysteresis phase loop; (b) PFM hysteresis amplitude loop; (c) PFM hysteresis loops of a wavy PZT ribbon on PDMS and a PZT film on Si, respectively. Comparison of piezoelectric and ferroelectric properties before and after transfer printing.

unique type of piezoelectric device architecture. To gain additional fundamental insights, we developed an analytical mechanics theory that is capable of capturing the physics of deformation and field response in such systems. In general, PZT is transversely isotropic with elastic, piezoelectric, and dielectric constants c_{ij}, e_{ij}, and k_{ij},[26] respectively. For a ferroelectric thin film, poled in the thickness direction (x_3) and subject to plane-stress deformation $\sigma_{33} = \sigma_{23} = \sigma_{13} = 0$ and vanishing in-plane electric fields $E_1 = E_2 = 0$, the in-plane stresses $\sigma_{\alpha\beta}$ and strains $\varepsilon_{\alpha\beta}$ ($\alpha,\beta = 1,2$) and out-of-plane electric field E_3 and displacement D_3 are related by $\sigma_{\alpha\beta} = (1 - \nu)\bar{E}\varepsilon_{\alpha\beta} + [\nu\bar{E}(\varepsilon_{11} + \varepsilon_{22}) - \bar{e}E_3]\delta_{\alpha\beta}$ and $D_3 = \bar{e}(\varepsilon_{11} + \varepsilon_{22}) + \bar{k}E_3$, where $\bar{E} = c_{11} - c_{13}^2/c_{33}$ is the plane-strain modulus, in-plane Poisson's ratio $\nu = (c_{12}c_{33} - c_{13}^2)/(c_{11}c_{33} - c_{13}^2)$, $\bar{e} = e_{31} - (c_{13}/c_{33})e_{33}$, and $\bar{k} = k_{33} + (e_{33}^2/c_{33})$.

For film widths that are much larger than the thickness (*i.e.*, the nanoribbon geometry), the strains in the width direction (x_2) are negligibly small, $\varepsilon_{22} = \varepsilon_{12} = 0$. Let ε_0 denote the membrane strain at the neutral plane ($x_3 = 0$) of the ferroelectric film, and κ the curvature due to buckling or bending, which both depend only x_1. The strain along the film direction (x_1) is $\varepsilon_{11} = \varepsilon_0 + \kappa x_3$. The dielectric governing equation $\partial D_3/\partial x_3 = 0$ gives $\bar{k}\partial E_3/\partial x_3 = -\bar{e}\kappa$. For a ferroelectric thin film of thickness h subject to electrical potential V between the top and bottom film surfaces, this gives the electrical field

$$E_3 = -\frac{V}{h} - \frac{\bar{e}}{\bar{k}}\kappa x_3 \qquad (1)$$

The PZT film stress and electric displacement can then be obtained as

$$\sigma_{11} = \bar{E}\left(\varepsilon_0 + \frac{\bar{e}V}{\bar{E}h}\right) + \bar{E}\left(1 + \frac{\bar{e}^2}{\bar{E}\bar{k}}\right)\kappa x_3 \qquad (2)$$

$$D_3 = \bar{e}\varepsilon_0 - \frac{\bar{k}V}{h} \qquad (3)$$

For a stiff thin film bonded to a compliant substrate, the effect of interface shear is negligible.[27] Force equilibrium then gives a constant axial force in the thin film (*i.e.*, $N = \bar{E}h\varepsilon_0 + \bar{e}V$), which implies that the membrane strain ε_0 does not vary with position. Prior to buckling the membrane strain ε_0 is zero since it is bonded to a thick, flat substrate. The axial force is $N = \bar{e}V$ is compressive because $\bar{e} < 0$ (*e.g.*, $\bar{e} = -7.5$ C/m^2 for PZT). As the electrical potential voltage V increases, the compressive stress eventually induces the thin film to buckle into a sinusoidal form represented by the out-of-plane displacement $u_3 = A\cos(2\pi x_1/\lambda)$, with buckling amplitude A and wavelength λ. The relation between membrane strain and displacements, $\varepsilon_0 = du_1/dx_1 + (du_3/dx_1)^2/2$ gives the in-plane displacement $u_1 = [\pi A^2/(4\lambda)]\sin(4\pi x_1/\lambda)$ and membrane strain $\varepsilon_0 = \pi^2A^2/\lambda^2$.

Minimization of the total energy $U_{\text{total}} = U_{\text{film}} + U_{\text{substrate}}$, $\partial U_{\text{total}}/\partial\lambda = \partial U_{\text{total}}/\partial A = 0$, gives the buckling wavelength

$$\lambda = 2\pi h\left[\frac{\bar{E}}{3\bar{E}_s}\left(1 + \frac{\bar{e}^2}{\bar{E}\bar{k}}\right)\right]^{1/3} \qquad (4)$$

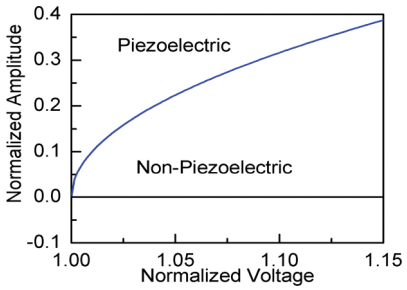

Figure 7. Calculated buckling amplitude A, normalized by $h(1 + \bar{e}^2/\bar{E}\bar{k})^{1/2}$, as a function of normalized voltage V/V_{crit} for wavy ribbons with and without piezoelectric effects.

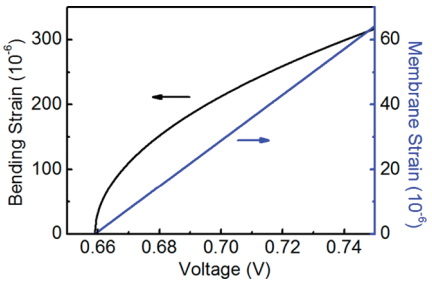

Figure 8. Calculated bending strain and membrane strain of wavy PZT ribbons as a function of applied voltage.

which is independent of electrical potential voltage V. The buckling amplitude is

$$A = h\left(1+\frac{\bar{e}^2}{\bar{E}\bar{k}}\right)^{1/2}\sqrt{\frac{V}{V_{crit}}-1} \text{ for } V \geq V_{crit} \quad (5)$$

which increases with V, where

$$V_{crit} = \frac{3\bar{E}_s h}{4|\bar{e}|}\left[\frac{\bar{E}}{3\bar{E}_s}\left(1+\frac{\bar{e}^2}{\bar{E}\bar{k}}\right)\right]^{1/3} \quad (6)$$

is the critical voltage for the thin film to buckle, and it is linearly proportional to the film thickness h. For the PDMS substrate $\bar{E}_s = 2.6$ MPa and PZT $c_{11} = 148$ GPa, $c_{12} = 76.2$ GPa, $c_{13} = 74.2$ GPa, $c_{33} = 131$ GPa, $e_{31} = -2.1$ C/m^2, $e_{33} = 9.5$ C/m^2, and $k_{33} = 2.08 \times 10^{-9}$ F/m,[14,28] the critical voltage is 0.66 V for the film thickness h = 100 nm. The buckling wavelength is linearly proportional to the film thickness h and so is the buckling amplitude for a fixed electric field V/h.

Figure 7 shows the buckling amplitude A, normalized by $h(1 + \bar{e}^2/\bar{E}\bar{k})^{1/2}$, *versus* the normalized voltage V/V_{crit} for wavy nanoribbon with piezoelectric and nonpiezoelectric effect, respectively. If the film has no piezoelectric effect, then the applied voltage cannot induce buckling. A universal curve results in the case of PZT because the elastic and piezoelectric properties and film thickness come into play only *via* the normalizations $h(1 + \bar{e}^2/\bar{E}\bar{k})^{1/2}$ and V_{crit}. This relation provides an approach to control the buckling amplitude *via* the voltage V, which is much different than the prestrain approach used in stretchable electronics.[14] It is important to note that the amplitude of a buckled ferroelectric film is several orders of magnitude larger than the lateral displacement obtained by the same ferroelectric film on a rigid substrate, which is given by $(e_{33}/c_{33})V$. For the PZT film, the amplitude in eq 5 is 536 and 745 times larger than the lateral displacement $(e_{33}/c_{33})V$ without buckling for the representative voltages of 0.70 and 0.75 V (and film thickness h = 100 nm), respectively. This significant increase of the lateral displacement may represent a useful way to take advantage of piezoelectricity in this way geometry.

Figure 8 shows the membrane strain $\varepsilon_0 = (|\bar{e}|/\bar{E}h)(V - V_{crit})$ and bending strain $\varepsilon_{bend} = [3\bar{E}_s h/(4|\bar{e}|V_{crit})]\sqrt{\varepsilon_0}$ in the wavy PZT nanoribbons. The maximum strains are $\varepsilon_0 \pm \varepsilon_{bend}$ (at the top and bottom surfaces of the nanoribbon), which range from −0.013 to −0.056% for the voltage V = 0.70 V (and film thickness h = 100 nm). As the voltage increases to 0.75 V, the strain ranges from −0.002 to −0.065%. These are very small as compared to the fracture strain of PZT.

CONCLUSIONS

The results presented here demonstrate processing schemes that allow fabrication of PZT nanoribbons in wavy forms on elastomeric substrates. From PFM measurements, the PZT nanoribbons integrated in this manner exhibit ferroelectricity and piezoelectricity comparable to related flat films on rigid silicon substrates. Theoretical analysis reveals the physics of these structures and provides certain predictions related to amplification effects in the displacement response and the ability to tune the structures with applied voltages. These results provide a foundation for future device-related work in this area.

EXPERIMENTAL METHODS

Fabrication of PZT Nanoribbons with Integrated Top and Bottom Side Electrodes. The top electrodes were patterned with photoresist (AZ nLoF 2070, Clariant), followed by deposition of Pt/Cr (150 nm/10 nm) using radio frequency sputtering on the surface of a multilayer stack of $Pb(Zr_{0.52}Ti_{0.48})O_3$/Pt/Ti/$SiO_2$ on a silicon wafer (400 nm/150 nm/10 nm/600 nm; INOSTEK) and liftoff in acetone. Inductively coupled plasma reactive ion etching (ICP-RIE) with Cl_2/Ar (20 sccm/5 sccm) through a hard mask of SiO_2 defined the lateral dimensions of PZT ribbons. The bottom electrode was patterned by ICP-RIE with a mask of a different size. Photolithographically patterned photoresist (AZ4620, Clariant) protected the PZT layers during removal of the sacrificial layer SiO_2 with dilute HF (deionized water (DI):52% HF = 1:2). For this procedure, a hard bake was conducted at 110 °C for 30 min. This protection step is crucial because PZT can also be

etched with HF. The square pads, under which the sacrificial layer SiO_2 are only partially removed due to their larger dimensions, located at the end of ribbons hold the PZT ribbons to prevent washing away into the etching bath until complete undercutting. Photoresist is removed in acetone after undercutting etching.

Transfer Process of PZT Nanoribbons onto PDMS Substrate. Gold electrodes were formed on the PDMS target substrate by electron beam evaporation through a shadow mask. Contacting a PDMS stamp against the PZT nanoribbons after undercut etching and the peeling the stamp away lifted the ribbons from the supporting silicon susbtrate, *via* fracture at their ends near the pad features (Figure 1). Prestrain was induced in a target PDMS substrate by controlled heating on a hot plate. Bringing the PDMS stamp, with arrays of PZT nanoribbons on its flat surface, against the heated PDMS, and then removing after ~10 min completed the process. Thermal expansion of the PDMS at 185 °C provided biaxial prestrains of ~5% . Wavy structures in the PZT nanoribbons form spontaneously after cooling to room temperature (~23 °C). The effective coefficienct of thermal expansion (CTE) of the stack is $\bar{\alpha}_{stack} = (2\bar{E}_{Pt}h_{Pt}\alpha_{Pt} + \bar{E}_{Cr}h_{Cr}\alpha_{Cr} + \bar{E}_{PZT}h_{PZT}\alpha_{PZT} + \bar{E}_{Ti}h_{Ti}\alpha_{Ti})/(\bar{E}_{stack}h_{stack})$ (~5.6 ppm/K), and the CTEs α_{Pt}, α_{Cr}, α_{PZT}, and α_{Ti} are 8.8, 4.9, 2.5, and 8.6 ppm/K, respectively.[22] The prestrain is estimated as ~5% from $(\alpha_{PDMS} - \bar{\alpha}_{stack})\Delta T$, where α_{PDMS} is 310 ppm/K and ΔT = 162 K.

Acknowledgment. Research supported by the U.S. Department of Energy Basic Energy Sciences Materials Science and Engineering Division (DEFG02-91ER45439) and performed at the Frederick Seitz MRL and Center for Microanalysis of Materials at the University of Illinois at Urbana—Champaign. X.F. acknowledges the support from the National Natural Science Foundation of China (Grant No. 10820101048). Y.H. acknowledges the support from ISEN, Northwestern University.

REFERENCES AND NOTES

1. Damjanovic, D. Ferroelectric, Dielectric and Piezoelectric Properties of Ferroelectric Thin Films and Ceramics. *Rep. Prog. Phys.* **1998,** *61*, 1267–1324.
2. Polla, D. L.; Francis, L. F. Processing and Characterization of Piezoelectric Materials and Integration into Microelectromechanical Systems. *Annu. Rev. Mater. Sci.* **1998,** *28*, 563–597.
3. Muralt, P. Piezoelectric Thin Films for MEMS. *Integr. Ferroelectr.* **1997,** *17*, 297–307.
4. Choi, J. J.; Park, G. T.; Park, C. S.; Kim, H. E. Ferroelectric and Piezoelectric Properties of Highly Oriented $Pb(Zr,Ti)O_3$ Film Grown on $Pt/Ti/SiO_2/Si$ Substrate Using Conductive Lanthanum Nickel Nitrate Buffer Layer. *J. Mater. Res.* **2005,** *20*, 726–733.
5. Tanimoto, T.; Okazaki, K.; Yamamoto, K. Tensile Stress—-Strain Behavior of Piezoelectric Ceramics. *Jpn. J. Appl. Phys.* **1993,** *32*, 4233–4236.
6. Wang, Z. L.; Song, J. H. Piezoelectric Nanogenerators Based on Zinc Oxide Nanowire Arrays. *Science* **2006,** *312*, 242–246.
7. Yang, R.; Qin, Y.; Li, C.; Zhu, G.; Wang, Z. L. Converting Biomechanical Energy into Electricity by a Muscle-Movement-Driven Nanogenerator. *Nano Lett.* **2009,** *9*, 1201–1205.
8. Xu, S.; Qin, Y.; Xu, C.; Wei, Y. G.; Yang, R. S.; Wang, Z. L. Self-Powered Nanowire Devices. *Nat. Nanotechnol.* **2010,** *5*, 366–373.
9. Qi, Y.; Jafferis, N. T.; Lyons, K.; Lee, C. M.; Ahmad, H.; McAlpine, M. C. Piezoelectric Ribbons Printed onto Rubber for Flexible Energy Conversion. *Nano Lett.* **2010,** *10*, 524–528.
10. Xu, S.; Hansen, B. J.; Wang, Z. L. Piezoelectric-Nanowire-Enabled Power Source for Driving Wireless Microelectronics. *Nat. Commun.* **2010,** *1*, 93.
11. Park, K.-I.; Xu, S.; Liu, Y.; Hwang, G.-T.; Kang, S.-J. L.; Wang, Z. L.; Lee, K. J. Piezoelectric $BaTiO_3$ Thin Film Nanogenerator on Plastic Substrates. *Nano Lett.* **2010,** *10*, 4939–4943.
12. Qi, Y.; Kim, J.; Nguyen, T. D.; Lisko, B.; Purohit, P. K.; McAlpine, M. C. Enhanced Piezoelectricity and Stretchability in Energy Harvesting Devices Fabricated from Buckled PZT Ribbons. *Nano Lett.* **2011,** *11*, 1331–1336.
13. Rogers, J. A.; Someya, T.; Huang, Y. Materials and Mechanics for Stretchable Electronics. *Science* **2010,** *327*, 1603–1607.
14. Khang, D. Y.; Jiang, H.; Huang, Y.; Rogers, J. A. A Stretchable Form of Single-Crystal Silicon for High-Performance Electronics on Rubber Substrates. *Science* **2006,** *311*, 208–212.
15. Kim, D.-H.; Ahn, J.-H.; Choi, W. M.; Kim, H.-S.; Kim, T.-H.; Song, J.; Huang, Y. Y.; Liu, Z.; Lu, C.; Rogers, J. A. Stretchable and Foldable Silicon Integrated Circuits. *Science* **2008,** *320*, 507–511.
16. Jiang, H.; Khang, D.-Y.; Song, J.; Sun, Y.; Huang, Y. Y.; Rogers, J. A. Finite Deformation Mechanics in Buckled Thin Films on Compliant Supports. *Proc. Natl. Acad. Sci. U. S.A.* **2007,** *104*, 15607–15612.
17. Kim, D.-H.; Song, J.; Choi, W. M.; Kim, H.-S.; Kim, R.-H.; Liu, Z.; Huang, Y. Y.; Hwang, K.-C.; Zhang, Y.-W.; Rogers, J. A. Materials and Noncoplanar Mesh Designs for Integrated Circuits with Linear Elastic Responses to Extreme Mechanical Deformations. *Proc. Natl. Acad. Sci. U.S.A.* **2008,** *105*, 18675–18680.
18. Kim, D.-H.; Xiao, J.; Song, J.; Huang, Y.; Rogers, J. A. Stretchable, Curvilinear Electronics Based on Inorganic Materials. *Adv. Mater.* **2010,** *22*, 2108–2124.
19. Park, J. C.; Hwang, S.; Kim, J.-M; Kim, J. K.; Yun, Y.-H.; Shim, K. B. Comparison of Chlorine and Fluorine-Based Inductively Coupled Plasmas for the Dry Etching of PZT Films. *J. Ceram. Process. Res.* **2009,** *10*, 700–704.
20. Koh, C. T; Liu, Z. J.; Khang, D.-Y; Song, J. Z.; Lu, C.; Huang, Y.; Rogers, J. A.; Koh, C. G. Edge Effects in Buckled Thin Films on Elastomeric Substrates. *Appl. Phys. Lett.* **2007,** *91*, 133113.
21. Song, J.; Jiang, H.; Liu, Z. J.; Khang, D. Y.; Huang, Y.; Rogers, J. A.; Lu, C.; Koh, C. G. Buckling of a Stiff Thin Film on a Compliant Substrate in Large Deformation. *Int. J. Solid Struct.* **2008,** *45*, 3107–3121.
22. Kaye, G. W. C.; Laby, T. H. *Tables of Physical and Chemical Constants*; Longman Scientific & Technical: New York, 1995.
23. Catalan, G.; Noheda, B.; McAneney, J.; Sinnamon, L. J.; Gregg, J. M. Strain Gradients in Epitaxial Ferroelectrics. *Phy. Rev. B* **2005,** *72*, 020102.
24. Lu, W.; Fang, D. N.; Li, C. Q.; Hwang, K. C. Nonlinear Electric-Mechanical Behaviour and Micromechanics Modelling of Ferroelectric Domain Evolution. *Acta Mater.* **1998,** *47*, 2913–2926.
25. Hwang, S. C.; Lynch, C. S.; McMeeking, R. M. Ferroelectric/Ferroelastic Interactions and a Polarization Switching Model. *Acta Metall. Mater.* **1995,** *4*, 2073–2084.
26. Parton, V. Z.; Kudryavtsev, B. A. *Electromagnetoelasticity*; Gordon and Breach Science Publishers: New York, 1988.
27. Huang, Z. Y.; Hong, W.; Suo, Z. Nonlinear Analyses of Wrinkles in a Film Bonded to a Compliant Substrate. *J. Mech. Phys. Solid* **2005,** *53*, 2101–2118.
28. Mitchell, J. A.; Reddy, J. N. A Refined Hybrid Plate-Theory for Composite Laminates with Piezoelectric Laminae. *Int. J. Solid Struct.* **1995,** *32*, 2345–2367.